Facile Exfoliation of Rectorite Nanoplatelets in Soy Protein Matrix and Reinforced Bionanocomposites Thereof

Jiahui Yu,[1,2] Guojuan Cui,[1] Ming Wei,[1] Jin Huang[1,3]

[1]*Joint Laboratory of Polymer Modification and Functional Materials, College of Chemical Engineering, Wuhan University of Technology, Wuhan 430070, China*
[2]*Institute of Biofunctional Materials and Devices, East China Normal University, Shanghai 200062, China*
[3]*Key Laboratory of Cellulose and Lignocellulosics Chemistry, Guangzhou Institute of Chemistry, Chinese Academy of Sciences, Guangzhou 510650, China*

Received 28 July 2006; accepted 30 November 2006
DOI 10.1002/app.25969
Published online 8 March 2007 in Wiley InterScience (www.interscience.wiley.com).

ABSTRACT: The rectorite (REC), a form of layered silicate, was facilely intercalated and even exfoliated in soy protein isolate (SPI) matrix. Furthermore, the reinforced biodegradable nanocomposite sheets were produced, in which the exfoliated REC lamellae plays a key role. After solution-mixing, XRD patterns showed that the REC lamellae were intercalated and even completely exfoliated for 4 wt % REC added, but the expanded gallery gradually became narrower with increasing REC content. FT-IR also verified the molecular-level associations between SPI molecules and REC lamellae by vibration variances of hydrogen bonding. The compression-molding further promoted intercalation and exfoliation, namely the 8 wt % REC can also be almost dispersed as exfoliated lamellae, while the interlayer of RECs also further separated for nanocomposites with higher REC content. TEM images visualized the transfer from exfoliation to intercalation and the decrease of interlayer distance with increasing REC content. The thicker and longer exfoliated REC lamellae resulted in high load and easy-to-yield of material. The maximum strength of nanocomposite sheets occurred at the addition of 12 wt % REC. Thereafter, the SPI chain can move more easily because of weak interaction between free negative-charge rich domain of SPI and REC surface in gallery, which did not favor enhancing mechanical performance. © 2007 Wiley Periodicals, Inc. J Appl Polym Sci 104: 3367–3377, 2007

Key words: soy protein; rectorite; biodegradable; nanocomposite; exfoliation; mechanical properties

INTRODUCTION

The layered silicate dispersing into polymer matrix as intercalation or exfoliation state usually resulted in the great improvement of performances over pristine polymer,[1] such as reinforcing materials,[2] reducing gas permeability,[3] enhancing thermal stability[4] and self-extinguishing fire-retardance,[5] and other interesting properties. As a result, the considerable attention is concentrated on exploring the mechanisms of intercalation and exfoliation in academic opinions and developing high performance and low-cost materials for meeting practical applications. Montmorillonite (MMT) is currently the most popular in the family of layered silicates,[6] and its nylon nanocomposite was taken as a representative example for reinforcing effect. It played a key role for the expansion of gallery distance and even exfoliation of lamellae that the metal cations, attached the interlayer surface with net negative charge of parallel stacking sandwiched lamella, can ion-exchange by the polar group of nylon.[7] At the same time, the strong interaction between the polar group of nylon and the negatively charged surface of lamella improved the compatibility among the components. In this process, the motion of polymer chains is of the foremost importance, which can be achieved from two dominant ways of solution[8] and melting intercalation.[9] Additionally, *in situ* intercalative polymerization can also exfoliate the stacking lamellae as gradual growth of polymer chains.[10] A great number of research has proven that the stronger interfacial bonding between the lamellae and matrix, and the homogeneous distribution of exfoliated lamella benefit higher mechanical strength.[1] To realize the exfoliation/delamination of layered silicates in com-

Correspondence to: J. Huang (huangjin@iccas.ac.cn).
Contract grant sponsor: National Natural Science Foundation of China; contract grant number: 20504010.
Contract grant sponsor: State Key Laboratory of Pulp and Paper Engineering, South China University of Technology; contract grant number: 200514.
Contract grant sponsor: Key Laboratory of Cellulose and Lignocellulosics Chemistry, Guangzhou Institute of Chemistry, Chinese Academy of Sciences; contract grant number: LCLC-2005-172.

posites, many strategies were submitted, such as organo-modification[11] and surface initiated polymerization[12] of layered silicates, polar group of polymer derivation[13] and compact polymer structure bearing multi polar groups (star,[14] dendritic,[15] and branched[16] structures).

With the claim of environmental protection and the lack of petroleum resource, soy protein has been used to produce eco-friendly plastics and adhesives[17] by virtue of its high rigidity and good adhesion ability combined with high performance, low-cost, and biodegradability characteristics. However, in the plasticization process of soy protein based-plastics to overcome brittleness and poor processablity,[18] it was put forward how to settle the significant decrease of its tensile strength. As a result, blending with other biodegradable polymers was extensively applied, and some candidates, such as polyphosphate,[19] polyester,[20] waterborne polyurethane,[21] polylactic acid,[22] chitin[23] and its whisker,[24] and so on, showed obvious reinforcing effects. In our previous practice,[25,26] the industrial lignins of different types were introduced, and the further improvements were realized by the reinforcement of cellulose[27] and compatibilization of reactive small molecule.[28] The results suggested that the strength of plasticized soy protein-based plastics was enhanced, and even the strength and elongation simultaneously increased in the blend of ligninsulphonate/soy protein.[25] Recently, the prominent reinforcing effects of nanometric scale and low loading content draw attentions to developing the soy-protein based bionanocomposite. Wei et al.[29] and Chen et al.[30] had enhanced the strength of soy protein plastics by virtue of the supramolecular nano-aggregates of hydroxylpropyl lignin. It was widely accepted that there existed the high affinity of clays to proteins and amino acids bearing neutral, positive, and even negative charges in soils.[31,32] Yu and coworkers[33,34] developed an effective and clean method to exfoliate the MMT lamellae in water under the assistance of ultrasonics, and then prepared the MMT-reinforced soy protein plastics plasticized by the mixture of water and glycerol. Thereby, Chen and Zhang[35] introduced MMT to significantly improve the strength and thermal stability of glycerol-plasticized soy protein plastics, and discovered that there existed strong hydrogen bonding and electrostatic interaction on the interface of soy protein and MMT. The increase of strength mainly attributed to the exfoliated MMT lamellae, which benefited from the structure of soy protein molecules and the whole process of treatment, that is, solution mixing and melting compression.[35]

Herein, another special layered silicate, rectorite (REC), was used to modify soy protein isolate (SPI) plastics. The REC is composed of a regular (1 : 1) stacking of mica-like layers and MMT-like layers.[36] Compared with the MMT interlayer spacing of about 1.2 nm, its interlayer spacing can reach about 2.4 nm. It is well-known that the narrow gallery is a main factor of restricting the insertion of polymer chains into layers because the higher gyration radius of typical polymers.[37] Thus, the REC was expected to allow soy protein molecules penetrating more availably, namely the REC lamellae are exfoliated more easily. In this work, we applied the methods of solution mixing and hot pressing to compound REC into SPI matrix, and the latter process would produce the molded sheets. The freeze-dried SPI/REC powders after solution mixing were characterized by Fourier transform infrared spectroscopy (FT-IR) and X-ray diffraction (XRD) to discover the original complex state in mixing solutions and the hydrogen bonding occurred at the surface of REC lamellae. Subsequently, the arrangements of REC in compression-molding sheet were studied by XRD patterns and the images of transmission electron microscope (TEM); as well the mechanical and thermal properties, and fractured surface of sheets were measured by tensile test, differential scanning calorimetry (DSC), and scanning electron microscope (SEM), respectively. On the basis of the testing results, the structure-properties relationships of such bionanocomposite sheets were further discussed.

EXPERIMENTAL

Materials

Commercial soy protein isolate (SPI) was purchased from DuPont-Yunmeng Protein Technology Co. (Yunmeng, China). The weight-average molecular weight (M_w) of SPI was determined by multi-angle laser light scattering instrument (MALLS, DAWN® DSP, Wyatt Technology Co., Santa Barbara, CA) equipped with a He-Ne laser ($\lambda = 632.8$ nm) to be 2.05×10^5.[29] The original moisture content, protein content, and amino acid compositions of SPI have been investigated and detailed in our previous paper, and the protein content of more than 90 wt % and 18 diverse amino acids were contained.[29] The rectorite (REC) with average size of $\sim$ 40 μm in length and 5 μm in width as well as cation exchange capacity of 40 meq/100 g was supplied by Hubei Celebrities Rectorite Technology Co. (Hubei, China). Glycerol purchased from the Shanghai Chemical Co. (Shanghai, China) was of analytical grade.

Preparation of nanocomposite powders

SPI (10 g) was dissolved in 160 mL distilled water at ambient temperature with mechanical stirring to obtain an emulsion. At the same time, a desired

amount of REC was dispersed in 40 mL distilled water and mechanical stirred for 30 min. Subsequently, the REC suspension was added into SPI emulsion with severe dispersing at 60°C for 2 h for producing the homogeneous blend. The resultant dark-gray viscous solutions were freeze-dried for 48 h to obtain a series of gray nanocomposite powders, which kept the original complex state in solution. According to the adding REC contents in solid powders of 0, 4, 8, 12, 16, 20, and 24 wt %, the nanocomposite powders obtained were coded as SR-0-P, SR-4-P, SR-8-P, SR-12-P, SR-16-P, SR-20-P, and SR-24-P, respectively. The nanocomposite powders were conditioned in a desiccator with silica gel as desiccant for 1 week at room temperature before characterization. The compositions and codes of nanocomposite powder were summarized in Table I.

Compression-molding of Sheets

The series of SR-P powders were mechanically mixed with the plasticizer of glycerol in an intensive mixer (Brabender, Germany), and the weight ratio of every solid powder and glycerol was controlled as 70 : 30 all the time. Subsequently, 5 g glycerol plasticized powders were compression-molded with 769YP-24B hot-press (Keqi High Technology Co., Tianjin, China) as the sheets at 140°C under the pressure of 20 MPa for 3 min, and then air-cooled to 50°C for half an hour before releasing the pressure for demolding. The dimension of the obtained sheets with the thickness of ~ 0.50 mm was about 70×70 mm^2. Corresponding to the original powders, the molded sheets were coded as the SR-0-S, SR-4-S, SR-8-S, SR-12-S, SR-16-S, SR-20-S, and SR-24-S, respectively. All the molded sheets containing REC showed a gray color and were less transparent due to the gray nature of REC as well as its greater dimension in the length and thickness of lamella. The nanocomposite sheets were conditioned in a desiccator with silica gel as desiccant for 1 week at room temperature before characterization, and their compositions and codes were listed in Table I.

TABLE I
The Compositions of Nanocomposite Powders and Sheets

Powder code	Solid composite W_{SPI} (wt %)	Solid composite W_{REC} (wt %)	Sheet code	Weight ratio of solid composite vs. glycerol
SR-0-P	100	0	SR-0-S	70 : 30
SR-4-P	96	4	SR-4-S	70 : 30
SR-8-P	92	8	SR-8-S	70 : 30
SR-12-P	88	12	SR-12-S	70 : 30
SR-16-P	84	16	SR-16-S	70 : 30
SR-20-P	80	20	SR-20-S	70 : 30
SR-24-P	76	24	SR-24-S	70 : 30

Characterization

X-ray diffraction (XRD) measurements were performed on a D8 Advance diffractometer (Bruker) equipped with a Cu Kα radiation source ($\lambda = 0.154$ nm). The diffraction data were collected in the range of $2\theta = 1$–10° using a fixed time mode with a step interval of 0.02°. The curves of Fourier transform infrared spectroscopy (FT-IR) were recorded on a 5700 spectrometer (Nicolet) in the range of 4000–400 cm^{-1} using a KBr-pellet method.

Scanning electron microscope (SEM) was carried out on a Hitachi X-650 scanning electron microscope. The sheets were frozen in liquid nitrogen and then snapped immediately. The fractured surfaces (the cross sections) of the films were sputtered with gold and then observed and photographed. Transmittance electron microscope (TEM) was performed with a FEI TecnaiG2 20 electron microscope at 180 kV. The ultrathin sections of the nanocomposite sheets were prepared by using a diamond knife on a Leica Ultracut UCT with EMFCS cryo-attachment at −120°C. The ultrathin sections with cross section thickness of 60 nm were directly placed on the copper grids for observation and photographing.

DSC analysis was carried out on a DSC-204 instrument (Netzsch, Germany) under nitrogen atmosphere at a heating or cooling rate of 20°C min^{-1}. The sheets were scanned in the range of −150 to 100°C after a pretreatment (heating from 20–100°C and then cooling down to −150°C) of eliminating the thermal history.

The tensile strength (σ_b), elongation at break (ε_b), and Young's modulus (E) of the sheets were measured on a universal testing machine (CMT6503, Shenzhen SANS Test Machine Co., Shenzhen, China) with a tensile rate of 5 mm min^{-1} according to GB13022-91. The tested samples were cut into the quadrate strips with the width of 10 mm, and the distance between testing marks was 40 mm. An average value of five replicates of each sample was taken.

RESULTS AND DISCUSSION

Structure of nanocomposite powders

The higher motion ability of polymer chains in solution can provide more possibility for the penetration into the gallery of REC. After solution mixing, the freeze-dried powders were investigated for the exfoliation of REC and the interfacial interaction between REC and SPI. XRD patterns, shown in Figure 1, indicated that the REC lamellae were intercalated and exfoliated functioned as adding content of REC, which was not perturbed by SPI because of no diffraction in the 2θ range of 1–10° for the SR-0-P without REC. Firstly, the separation of REC lamellae was proved by the disappearance of two dominant peaks located at 3.64° (2.43 nm) and 7.16° (1.10 nm),

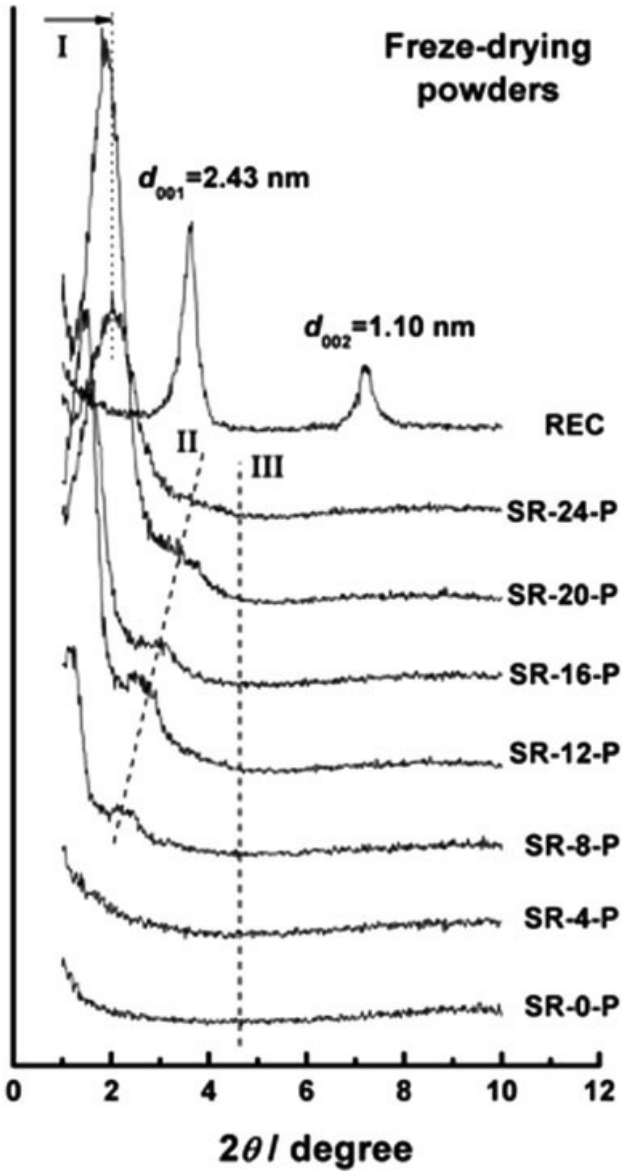

Figure 1 XRD patterns of the freeze-drying nanocomposite powders from the mixing solutions with different REC contents, as well as REC powder and the freeze-drying SPI powder.

assigned to the d_{001} and d_{002} of REC.[36] When a small amount (4 wt %) of REC was added, the SR-4-P showed highly disordered with no diffraction peak. It suggested that the layered stacking of REC lamellae were destroyed and dispersed into the SPI matrix as isolated nanoplatelets, namely the REC was almost completely exfoliated. However, the increase of REC content resulted in the occurrence of low-angle diffraction peaks, such as a weak diffraction at about 2.17° for SR-8-P. As the REC content was higher than 8 wt %, the nanocomposite powders had a dominant peak at about 1.16–2.02° except for weak diffraction mentioned above. Interestingly, the peak positions and weak diffractions shifted to wider angle with increasing REC content. The tested data and corresponding *d*-spacing, summarized in Table II, suggested that the expanded distance of REC gallery gradually became narrower, that is, the *d*-spacing decreased from 7.62 nm in the SR-8-P to 4.38 nm in the SR-24-P. Such results were in agreement with the conclusion raised by Ray and Okamoto about the dependence of the nanocomposite structure (exfoliation or intercalation) on the content of layered silicate.[38] Even though the XRD patterns of nanocomposite powders containing higher loading showed predominant intercalation character, the REC lamellae were inevitably exfoliated. In any case, the solution mixing have successfully made the SPI molecules penetrate into the REC gallery, and then the intercalated and even exfoliated nanocomposites were produced without other special aids.

Interaction in nanocomposite powders

It was well-known that the surface character of REC lamellae was similar to montmorillonite (MMT). As a result, the SPI molecules can strongly adhere onto the surface of REC lamellae by electrostatic affinity and hydrogen bonding. According to the basic understanding of electrostatic interaction in SPI/MMT nanocomposites,[35] the net negative-charge SPI, directed by the ion-exchange of its positive-charge rich domain with the surface cations of REC lamellae, can penetrate into the REC gallery to broaden the interlayer distance and even cause complete separation. Although the highly exfoliated REC lamellae can anchor by the positive-charge rich domain of SPI, the exclusion between the negative-charge rich domain and negative-charge lamellae surface after ion-exchanging diminished the contact area between the REC lamellae and SPI molecules, especially for the SPI molecules in expanded gallery. When the electrostatic interaction induced the affinity of SPI onto REC lamellae, the hydrogen-bonds formed between C=O and —NH in SPI and Si—O—Si and —OH groups on REC lamella.[39] Herein, only simple FT-IR measurement was applied to discover the molecular-level contact between REC and SPI, and discuss the effects of REC content on intercalation or

TABLE II
The 2θ Angles and Corresponding *d* Values of Nanocomposite Powders

	Character I		Character II	
Sample	2θ (degrees)	*d* (nm)	2θ (degrees)	*d* (nm)
SR-4-P	–	–	–	–
SR-8-P	1.16	7.62	2.17	4.08
SR-12-P	1.45	6.10	2.48	3.57
SR-16-P	1.64	5.39	2.90	3.05
SR-20-P	1.85	4.78	3.35	2.64
SR-24-P	2.02	4.38	3.60	2.46

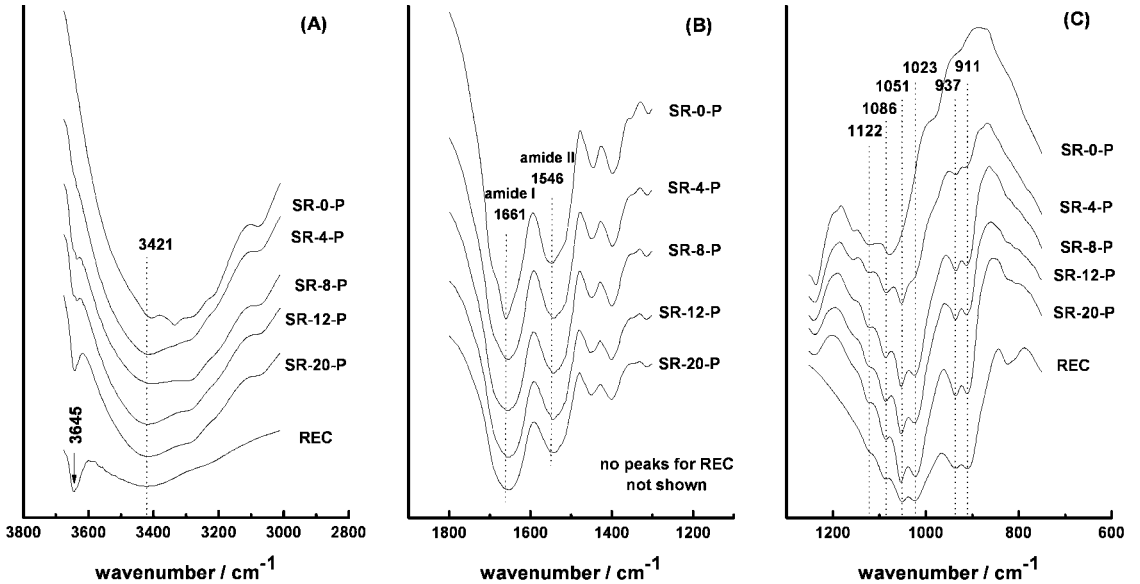

Figure 2 Three FT-IR regions of 3750–3000 cm^{-1} (A), 1800–1400 cm^{-1} (B) and 1300-950 cm^{-1} (C) for the freeze-drying nanocomposite powders, as well as the powders of REC and SR-0-P without REC.

exfoliation. Three FT-IR regions of the 3750–3000 cm^{-1}, 1800–1400 cm^{-1}, and 1300–950 cm^{-1}, were depicted in Figure 2 for complex powders as well as REC and SR-0-P without REC. The positions and assignments of characteristic peaks were listed in Table III.

Figure 2(A) showed the O—H stretching (3645 and 3421 cm^{-1}) onto REC[40] and N—H and O—H stretching in SPI with multi-peaks. The increasing intensity of peak at 3645 cm^{-1} was good agreement with the increase of REC content. Although the bands of SPI partly overlapped by the peak at 3421 cm^{-1} of REC, it can be clearly identified that the absorption of SPI shifted down to low frequency as well the intensity increased, indicating that the stronger hydrogen bonding associated with —NH and —OH in SPI formed after introducing REC. Such result can be also verified by the shift to low frequency and increasing intensity of amide II (N—H bending and C—N stretching modes) in Figure 2(B) functioned as the increase of REC content. Although the amide I (C=O stretching) band at 1661 cm^{-1} shifted to low frequency, its vibration intensity became weaker with increasing REC, while the absorbance located at higher wavenumber (free C=O) became stronger. It can be explained that the original interaction in SPI may be destroyed after adding REC, while new hydrogen bonds associated with C=O in SPI formed. Additionally, there existed three groups of vibrations in Figure 2(C), that is, in-plane Si—O stretching (1122, 1051, and 1023 cm^{-1}), out-of-plane Si—O stretching (1086 cm^{-1}) and O—H bending (937 and 911 cm^{-1}) onto REC lamella. In spite of no changes of in-plane Si—O stretching, the relatively intensity of two bands for O—H bending obviously changed with increasing REC content, indicating that —OH on the surface of REC lamellae participated the formation of hydrogen bonding between SPI molecules and REC lamellae. It is noted that the out-of-plane Si—O stretching associated with the orientation of silicate layers, that is, its intensity increased with increasing disordered extent of lamellae arrangement.[41] As a result, the increasing intensity at 1086 cm^{-1} for complex powders, compared with the pure REC powder, suggested that the REC lamellae were exfoliated and disorderly dispersed into SPI matrix. However, the intensity of out-of-plane Si—O stretching did not continuously increased with increasing REC content. When the REC content was higher than 12 wt %, the relative intensity of peak at 1086 cm^{-1} decreased, suggesting that the exfoliation of REC lamellae was hindered in the complex powders containing excess REC. It was

TABLE III
The Positions and Assignments of Characteristic Peaks for Nanocomposite Powders As Well As REC Powder and SR-0-P without REC Measured by FT-IR

Sample	Wavenumber (cm^{-1})	Assignment
REC	3645 and 3421	O—H stretching
	1122, 1051, and 1023	In-plane Si—O stretching
	1086	Out-of-plane Si—O stretching
	937 and 911	O—H bending
SPI	3600–3200	N—H and O—H stretching
	1661	Amide I (C=O stretching)
	1546	Amide II (N—H bending and C—N stretching)

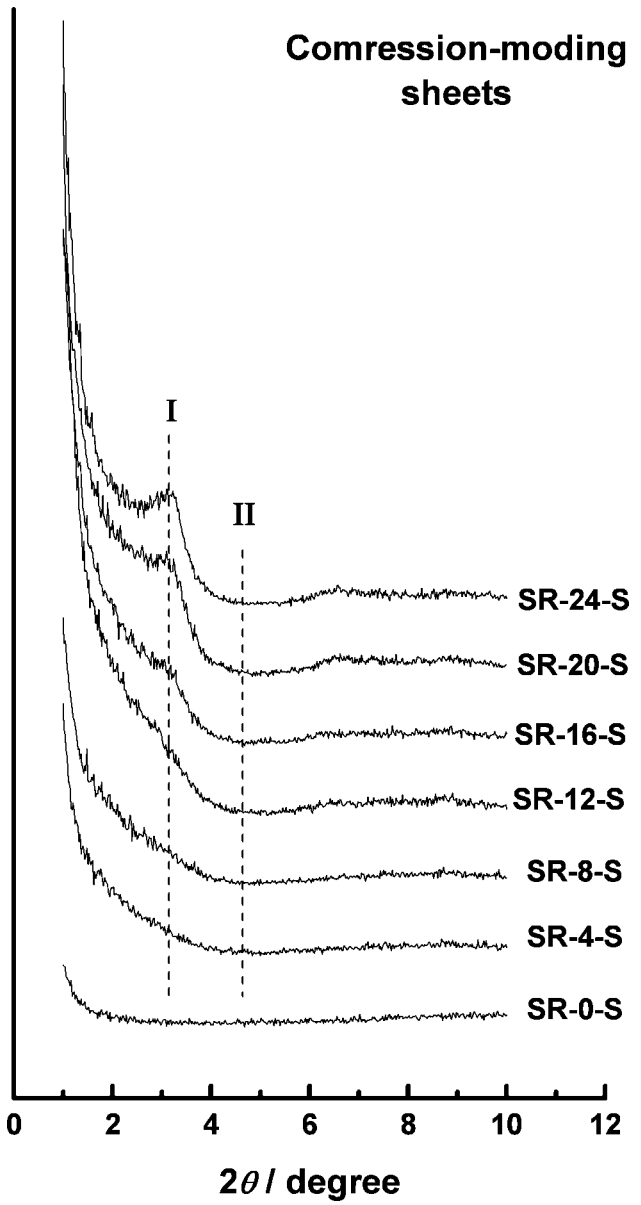

Figure 3 XRD patterns of the compression-molding nanocomposite sheets from the freeze-dried powders with different REC contents.

just 12 wt % REC loading to provide maximum exfoliated lamellae that disorderly dispersed. It not only consists with the XRD results, but further evaluates exfoliated extent in complex exfoliation/intercalation state.

The FT-IR results on hydrogen bonding in nanocomposite powders can be summarized as: the hydrogen bonding associated with —NH of SPI was improved; new hydrogen bonds associated with C=O of SPI formed after introducing REC destroyed the original interaction in SPI matrix; the —OH on the surface of REC lamellae participated in the formation of new hydrogen bonds. Thus, it is believed that the hydrogen bonding formed at H atom in N—H of SPI and O atom on the REC surface as well as H atom in O—H on the REC surface and polar groups of SPI. However, these changes in FT-IR spectra were more and more unobvious as the REC content was higher than 12 wt %. Combined with the XRD results, it resulted from the restriction of exfoliated structure while the intercalated structure appeared and increased with increasing REC content. In the intercalated gallery of REC, the SPI molecules cannot adhere onto the surface of REC lamellae and then resulted in no obvious enhancement of hydrogen bonding at the interface of SPI matrix and REC lamellae.

Structure of REC in nanocomposite sheets

With the plasticization of 30 wt % glycerol, the SPI/REC plastics have been obtained through a compression-molding process. The XRD patterns of the nanocomposite sheets containing various REC contents were depicted in Figure 3. Obviously, the dominant peaks in XRD patterns of nanocomposite powders, assigned to the intercalated structure, disappeared or became weaker. Especially, the REC in SR-8-S was almost exfoliated as well, proved by the patterns, similar to SR-4-P and SR-4-S, with no diffraction. This result suggested that the REC lamellae were further delaminated in the melting-compression process. However, the complete exfoliation cannot be realized for the complex sheets with higher loading of REC. A weak diffraction located at 3.14° (2.82 nm) occurred for the nanocomposite sheets with the REC content higher than 12 wt % and became stronger with increasing REC content. Although the melting compression promoted the delamination of REC lamellae, some intercalated structure remained in the nanocomposite sheet.

TEM images in Figure 4 visualized the morphology of REC lamellae in the nanocomposite sheets. As shown in Figure 4(A) of SR-4-S, the REC lamellae existed in SPI matrix as the exfoliated state. At the same time, the lamellae stacking can be observed in Figure 4(B) of SR-12-S and Figure 4(C) of SR-20-S as well as the dispersion of single lamella to some extent. However, even though both were the intercalated structures, the interlayer distances were obviously different as well as the thickness and number of lamellae stacking. As the REC content increased, the interlayer distance decreased from 6.06 nm of SR-12-S to 4.68 nm of SR-20-S, while the number and thickness of lamella stacking increased. Compared with the statistical results from XRD, the TEM images further visualized fine structures of REC lamellae in SPI matrix and described the faint differences under changing REC content. In addition, the longer and thicker character of REC lamellae may contribute to high loading, easy-to-bending, and high strength.

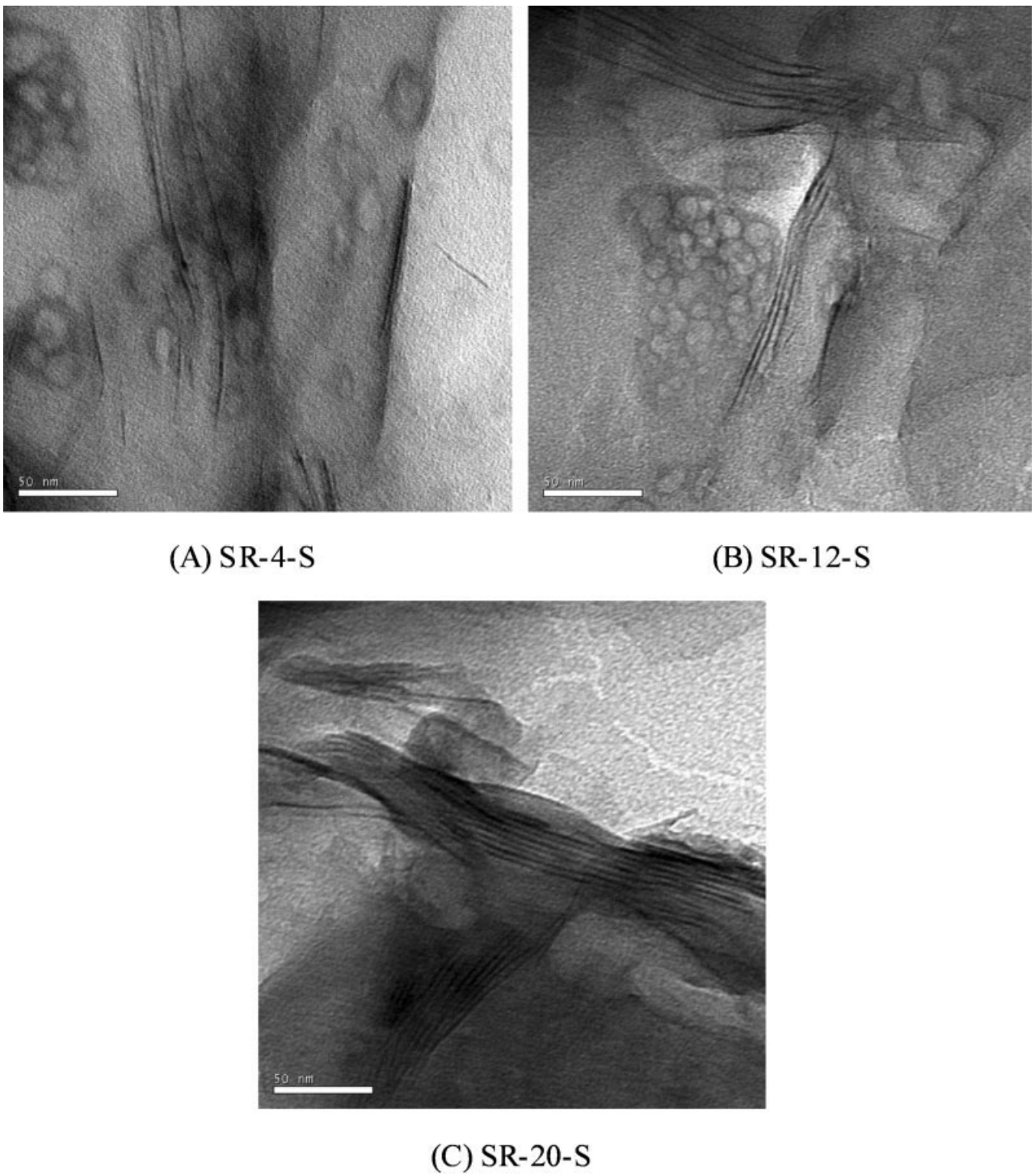

Figure 4 TEM images of the ultrathin sections from compression-molding nanocomposite sheets with the REC contents of 4 wt % (A, SR-4-S), 12 wt % (B, SR-12-S), and 20 wt % (C, SR-20-S).

Mechanical properties of nanocomposite sheets

As expected, adding REC obviously reinforced the SPI materials. Figure 5 showed the effects of REC content on the mechanical properties, including tensile strength (σ_b), Young's modulus (E), and elongation at break (ε_b). The tensile strength of the SR-S sheets was firstly enhanced from 6.82 MPa (SR-0-S only containing SPI) to 12.92 MPa (the adding content of 12 wt % REC), and then gradually decreased. The enhancement of strength is mainly attributed to the exfoliated REC lamellae and stronger interfacial interaction. But weak interfacial affinity in interca-

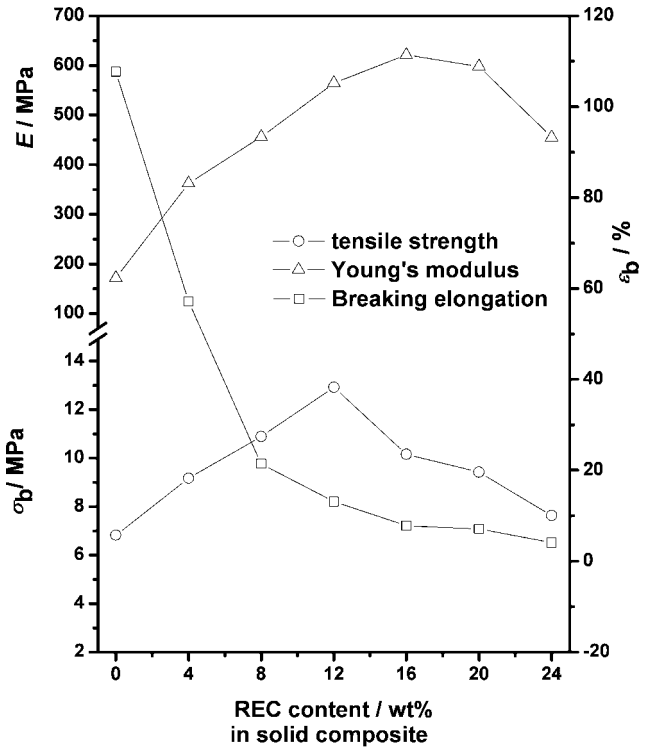

Figure 5 Effects of REC contents on tensile strength (σ_b), elongation at break (ε_b) and Young's modulus (E) for the nanocomposite sheets.

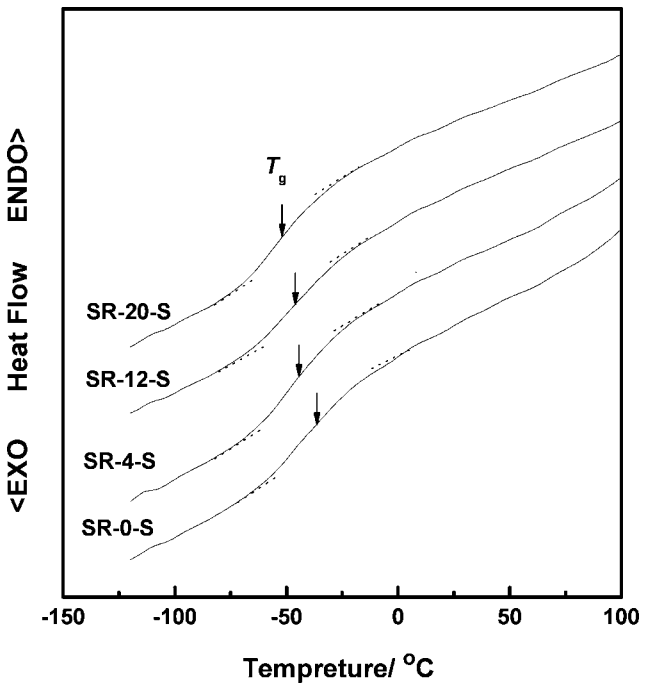

Figure 6 DSC thermograms of the nanocomposite sheets containing 4 wt % (SR-4-S), 12 wt % (SR-12-S), and 20 wt % (SR-20-S) REC as well as the pure SPI sheet (SR-0-S).

lated gallery, formed under higher REC loading, damaged the mechanical properties, shown as the decrease of strength. Although the SR-12-S was verified by TEM images to containing a fraction of intercalated structure, more exfoliated REC lamellae produced higher strength yet. It was well consistent with the FT-IR results of powders, that is, there were maximum exfoliated REC lamellae disorderly dispersed into SPI matrix for the SR-12-S containing 12 wt % REC even though the intercalated structure was easily observed and also became more and more. However, when the REC content was higher than 16 wt %, the exfoliation was restricted due to too higher loading. The intercalated structures sharply increased and damaged the mechanical performance.

The Young's modulus presented a tendency of changes similar to the tensile strength, but the maximum value of 621.01 MPa occurred at the REC content of 16 wt %, which was 3.6 times of modulus of pure SPI sheet (SR-0-S). The Young's modulus generally represents the rigidity of material. Herein, the enhancement of Young's modulus was not necessarily determined by intercalated or exfoliated states of REC lamellae. Once the REC was introduced, the damage to original SPI structure was inevitable. As a result, the initial increases of modulus attributed to relatively higher rigidity of inorganic fillers, and the decrease of modulus after adding higher than 16 wt % REC resulted from the excessive destroy of original structure in SPI matrix. However, the elongation of nanocomposite material was more sensitive to such damage of original structure in SPI matrix. The elongation at break of nanocomposites sheets sharply decreased with increasing REC content and the sheets containing REC contents higher than 16 wt % were very easily ruptured in the tensile mode.

Thermal properties and fractured morphology of sheets

The glass transition is the process from glassy state to rubbery state, and associated with the initial motion of polymer chains at the molecular level. As a result, the glass transition temperature (T_g) was generally used to discover the differences of chemical environments in composite materials, such as intermolecular interaction, spatial hindrance, and so on. Herein, the SPI sheets with or without REC were measured by DSC, and the thermograms and data of

TABLE IV
The Data of Glass Transition for the Sheets with and without REC

Sample	$T_{g,\text{onst}}$ (°C)	$T_{g,\text{mid}}$ (°C)	$T_{g,\text{end}}$ (°C)	ΔC_p (J g^{-1} K^{-1})
SR-0-S	−59.3	−36.6	−13.8	0.641
SR-4-S	−65.4	−44.5	−23.5	0.640
SR-12-S	−69.3	−45.7	−22.1	0.617
SR-20-S	−71.9	−52.0	−32.0	0.605

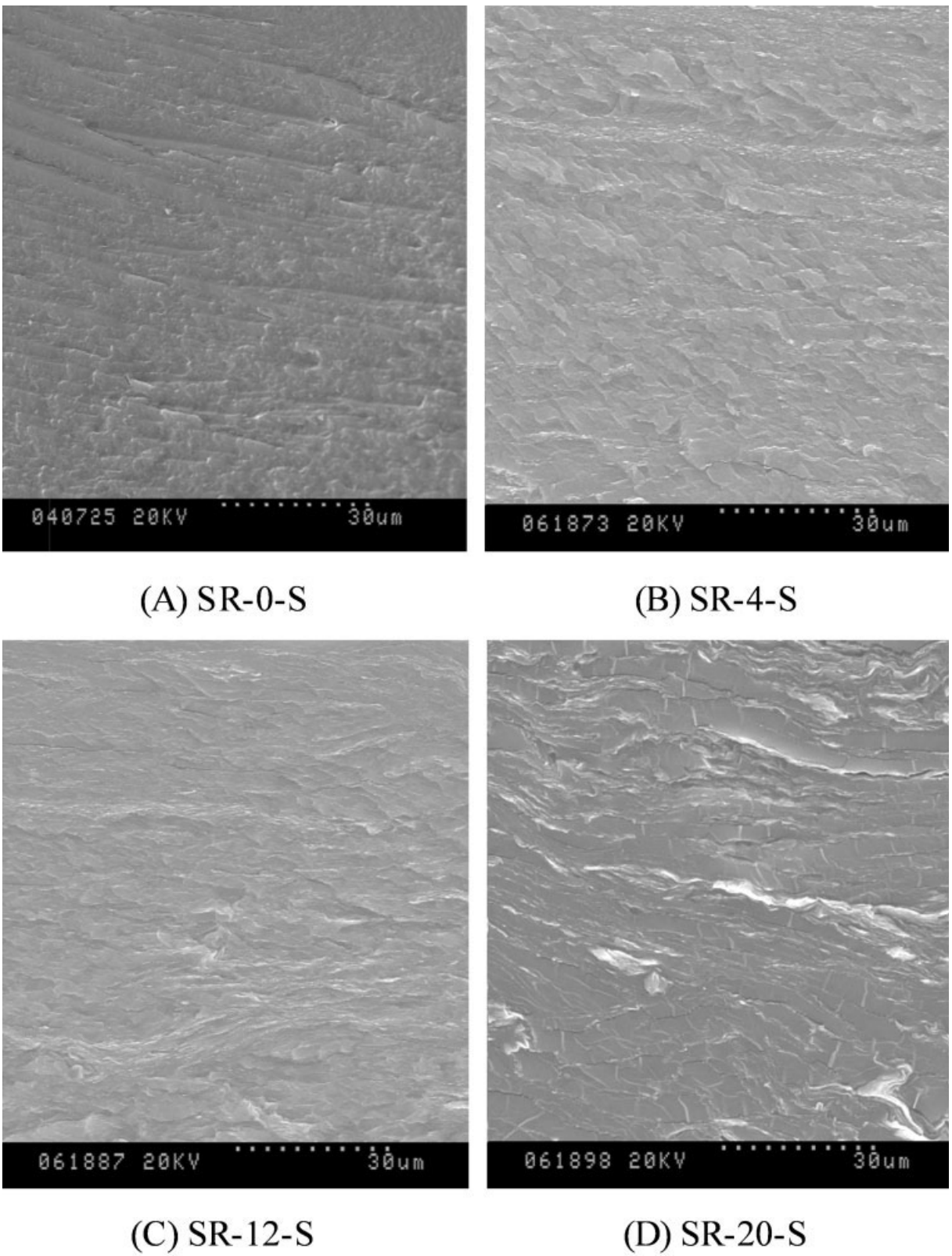

Figure 7 SEM images of the fractured surfaces from compression-molding sheets without REC (A, SR-0-S) and with the REC contents of 4 wt % (B, SR-4-S), 12 wt % (C, SR-12-S), and 20 wt % (D, SR-20-S).

T_g and heat-capacity increment (ΔC_p) were depicted in Figure 6 and Table IV, respectively. It is obvious that the T_g at onset and midpoint and ΔC_p were decreased with increasing REC content, indicating that the SPI chains have more freedom of motion. If only considering the stronger interaction at the

interface of SPI matrix and REC lamella, the motion of SPI should be restricted with T_g increasing. However, the FT-IR results suggested that the original structure and hydrogen bonding in SPI matrix was destroyed after introducing REC. Additionally, it was proposed that only positive-charge rich domains of SPI can strongly adhere the exfoliated lamella of layered silicate, while the negative-charge rich domains were relatively free as well as no strong affinity in the expanded gallery of stacking lamellae.[35] These factors directly provided the higher freedom of SPI chains and resulted in the decrease of T_g and ΔC_p even though some SPI molecules were restricted into the REC gallery.

The SEM images of fractured surface for nanocomposite sheets were shown in Figure 7. The heterogeneous morphology of SR-0-S without REC [Fig. 7(A)] originated from the complex component and structure in soy protein, such as globin domain, amorphous domain and so on.[29] However, 4 wt % REC as almost exfoliated state in SPI matrix resulted in appearance of some small plate-like morphology in Figure 7(B), showing an obvious brittle-fractured character. As the REC content increased, the brittle-fracture became more and more obvious, but represented other morphology due to the increase of intercalated structure. The SR-12-S sheet in Figure 7(C) showed striation structures, which was just occupied by the lamellae stacking in the naocomposite sheet. XRD and TEM results proved that the continuous increase of REC content caused more intercalated structures and narrower interlayer distance. As a result, the SR-20-S sheet showed heterogeneous dispersion of more striation structures and large-area smooth surface, resulting from the removal of small and large lamellae stacking after fractured. These results not only depicted a brittle-fractured character of elongation decrease, but pointed out that the modulus decrease may result from inhomogenous distribution of intercalated or exfoliated lamellae at high loading of REC.

CONCLUSIONS

The REC was highly exfoliated and intercalated in SPI matrix depending on the characteristic structure of REC and SPI as well as the motion ability of molecular chain provided by the process of solution mixing and melting compression. At the same time, the exfoliated REC lamellae resulted in enhancement of strength and modulus of SPI plastics, which may dissolve the shortcoming of plasticization to some extent. The highest strength happened on 12 wt % REC loading, which reached 12.92 MPa by almost twice of pure SPI plastics. The possible mechanism of facile exfoliation in REC filled SPI nanocomposite was proposed, namely the strong affinity of positive-charge rich domain onto SPI matrix as well as the hydrogen bonding. However, high REC loading did not benefit the exfoliation of lamellae, and the intercalated structures gradually dominated while the interlayer became narrower with an increase of REC content. On the basis of the structure and interaction analysis, the reinforcing effects resulted from the strong interfacial interaction between SPI and exfoliated REC lamellae even though the original structure and interaction in SPI matrix were partly destroyed. The intercalated structures cannot produce the optimal mechanical performances for SPI plastics, especial for the nanocomposite with high REC content, due to relatively poor interfacial adhesion and inhomogenous distribution.

References

1. Usuki, A.; Hasegawa, N.; Kato, M. Adv Polym Sci 2005, 179, 135.
2. Chen, B.; Evans, J. R. G. Macromolecules 2006, 39, 747.
3. Messersmith, P. B.; Giannelis, E. P. J Polym Sci: Part A: Polym Chem 1995, 33, 1047.
4. Ma, X.; Liang, G.; Liu, H.; Fei, J; Huang, Y. J Appl Polym Sci 2005, 97, 1915.
5. Zhu, J.; Morgan, A. B.; Lamelas, F. J.; Wilkie, C. A. Chem Mater 2001, 13, 3774.
6. Kojima, Y.; Usuki, A.; Kawasumi, M.; Okada, A.; Kurauchi, T.; Kamigaito, O. J Polym Sci: Part A: Polym Chem 1993, 31, 983.
7. Usuki, A.; Kawasumi, M.; Kojima, Y.; Okada, A.; Kurauchi, T.; Kamigaito, O. J Mater Res 1993, 8, 1174.
8. Burnside, S. D.; Giannelis, E. P. Chem Mater 1995, 7, 1597.
9. Pluta, M.; Paul, M.; Alexandre, M.; Dubois, P. J Polym Sci Part B: Polym Phys 2006, 44, 299.
10. Yoo, Y.; Choi, K.; Lee, J. H. Macromol Chem Phys 2004, 205, 1863.
11. LeBaron, P. C.; Wang, Z.; Pinnavaia, T. Appl Clay Sci 1999, 15, 11.
12. Pollet, E.; Delcourt, C.; Alexandre, M.; Dubois, P. Macromol Chem Phys 2004, 205, 2235.
13. Vaia, R. A.; Vasudevan, S.; Krawiec, W.; Scanlon, L. G.; Giannelis, E. P. Adv Mater 1995, 7, 154.
14. Robello, D. R.; Yamaguchi, N.; Blanton, T.; Barnes, C. J Am Chem Soc 2004, 126, 8118.
15. Costa, A. S.; Imae, T.; Takagi, K.; Kikuta, K. Prog Colloid Polym Sci 2004, 128, 113.
16. Bae, W. J.; Kim, K. H.; Jo, W. H. Macromolecules 2004, 37, 9850.
17. Kumar, R.; Choudhary, V.; Mishra, S.; Varma, I. K.; Mattiason, B. Ind Crops Prod 2002, 16, 155.
18. Zhang, J.; Mungara, P.; Jane, J. Polymer 2001, 42, 2569.
19. Otaigbe, J. U.; Adams, D. O. J Environ Polym Degrad 1997, 5, 199.
20. Graiver, D.; Waikul, L. H.; Berger, C.; Narayan, R. J Appl Polym Sci 2004, 92, 3231.
21. Wang, N.; Zhang, L.; Gu, J. J Appl Polym Sci 2005, 95, 465.
22. Zhang, J.; Jiang, L.; Zhu, L.; Jane, J.; Mungara, P. Biomacromolecules 2006, 7, 1551.
23. Zheng, H.; Tan, Z.; Zhan, Y.; Huang, J. J Appl Polym Sci 2003, 90, 3676.
24. Lu, Y.; Weng, L.; Zhang, L. Biomacromolecules 2004, 5, 1046.
25. Huang, J.; Zhang, L.; Chen, F. J Appl Polym Sci 2003, 88, 3284.
26. Huang, J.; Zhang, L.; Chen, P. J Appl Polym Sci 2003, 88, 3291.

27. Huang, J.; Zhang, L.; Wang, X. J Appl Polym Sci 2003, 89, 1685.
28. Huang, .J; Zhang, L.; Wei, H.; Cao, X. J Appl Polym Sci 2004, 93, 624.
29. Wei, M.; Fan, L.; Huang, J.; Chen, Y. Macromol Mater Eng 2006, 291, 524.
30. Chen, P.; Zhang, L.; Peng, S.; Liao, B. J Appl Polym Sci 2006, 101, 334.
31. De Cristofaro, A.; Violante, A. Appl Clay Sci 2001, 19, 59.
32. Newman, S. P.; Di Cristina, T.; Coveney, P. V. Langmuir 2002, 18, 2933.
33. Dean, K.; Yu, L. In Biodegradable Polymers for Industrial Applications; Smith R., Ed.; CRC Press: Boca Raton, FL, 2005.
34. Yu, L.; Dean, K.; Li, L. Prog Polym Sci 2006, 31, 576.
35. Chen, P.; Zhang, L. Biomacromolecules 2006, 7, 1700.
36. Grim, R. E. Clay Mineralogy; McGraw-Hill: New York, 1968.
37. Balazs, A. C.; Singh, C.; Zhulina, E.; Lyatskaya, Y. Acc Chem Res 1999, 32, 651.
38. Ray, S. S.; Okamoto, M. Prog Polym Sci 2003, 28, 1539.
39. Sohn, J. R.; Kim, J. T. Langmuir 2000, 16, 5430.
40. Bougeard, D.; Smirnov, K. S.; Geidel, E. J Phys Chem B 2000, 104, 9210.
41. Ras, R. H. A.; Johnston, C. T.; Franses, E. I.; Ramaekers, R.; Maes, G.; Foubert, P.; De Schryver, F. C.; Schoonhertdt, R. A. Langmuir 2003, 19, 4295.